Reflection and Rotation for Three Dimensional Microscopy of Live Cells

Charlie Wright

Advisor: John Wikswo

April 18, 2008

TABLE OF CONTENTS

ABSTRACT

Confocal scanning laser microscopy and multiphoton microscopy provide 3D data from biological specimens, but with limited z-axis precision. Multiple microscale mirrors can be used to obtain more accurate 3D data on living cells while using classical widefield microscopy. Etched silicon wells coated with aluminum were used to obtain 3D images of budding yeast cells, with information along the z-axis provided by reflections from the angled sides of the well. To supplement measurements obtained with this method, work was also conducted on a system to allow for rotation of a cell attached to a pulled glass tip. Images of a yeast cell obtained from either method can be fit to a simple 3D surface due to the cell's roughly spheroidal shape, which should provide accurate measurements of the volume of an individual budding yeast cell as it progresses through the cell cycle.

INTRODUCTION

Microscopy in Three Dimensions

Biological phenomena exist in all three spatial dimensions, and a three dimensional (3D) description of biological events, especially morphological processes, is necessary for an understanding of their functions. However, microscopy usually provides images within a single focal xy plane at a specific position along the z-axis, resulting in two dimensional (2D) images. Advances in imaging technology in recent decades have allowed the collection of 3D images, with important repercussions for the microscopy of cells and subcellular objects. The most common techniques for generating 3D data are implementations of optical sectioning microscopy (OSM), which slice through a slab of the specimen and use various methods to eliminate out-of-focus light. A composite stack of images taken at different depths can then provide information about 3D structure.

In confocal laser scanning microscopy (CLSM), illumination of a specimen is confined to a diffraction-limited spot and detection is also confined to this spot, so that signal from a fluorescent point falls off with an approximate inverse fourth-power law with distance from the plane of focus. Glare from out-of-focus regions is thus reduced and 3D information can be built up by rapidly scanning an illuminated spot at different focal planes (Amos and White 2003). A related technique is deconvolution microscopy, which uses a computational method to reduce out-of-focus fluorescence, and which has the advantage of functioning at very low light levels (McNally *et al.* 1999). Multiphoton laser scanning microscopy (MPLSM) diminishes unwanted fluorescence by using a high peak-power, pulsed laser to illuminate the specimen with a wavelength about twice that

of the absorption peak of the fluorophore, resulting in excitation of fluorophores in the focal plane (Denk *et al.* 1990). A variation on the theme of optical sectioning through selective fluorescence is tilted view microscopy (TVM), which reorients fixed samples relative to the optical axis to obtain cross-sections with high in-plane resolution that can be recombined into a 3D model (Shaw *et al.* 1989).

OSM techniques have revolutionized modern microscopy by increasing z-resolution to allow generation of complex sets of 3D data. For example, CLSM can achieve a maximum z-resolution of 0.5 µm, whereas optimal resolutions of 2-3 µm are obtained with widefield microscopy (Ziegler *et al.*). Nevertheless, this falls short of the maximal xy resolution available for CLSM of about 0.2 µm (Prasad et al. 2007). High-quality images are also more difficult to obtain with these methods than with conventional techniques, and thus they are highly user-dependent (Conchello and Lichtman 2005). TVM is also limited by exact alignment requirements and the need for a fixed specimen (Seale *et al.*, submitted). In addition, challenges remain in data storage and acquisition, and in cost-effectiveness (Rueden and Eliceiri 2007).

This project investigated two alternate techniques for 3D imaging of live cells. The first involves a system of microscale mirrors, termed mirrored pyramidal wells (MPWs), which provide z-axis information through reflections of an object placed within them. Each well is constructed such that it contains four angled mirrored sides and a flat mirrored bottom. An object placed within the well

Fig. 1. A dice in a mirrored well. Information about each of the six faces is available.

generates four reflections from the sides and one from the bottom, as illusrated in Fig. 1. This provides a convenient method of simultaneously obtaining optical slices through a specimen to give information along the z-axis which is not available in an image taken from a single vantage point. As opposed to most OSM techniques, the slices given by the reflections from the sides are nearly orthogonal. Unlike those methods which take slices at each focal depth, MPWs reorient the point spread function, the 3D intensity pattern of a point source of light near the focal plane, to obtain more accurate information along an axis nearly orthogonal to the focal plane. Unlike TVM, little calibration is required, as the geometry of the mirrored wells can be completely determined from their dimensions along the top and bottoms sides. Information given by the reflections can be used to reconstruct a model of an object in 3D with more accuracy than that available for conventional 2D microscopy.

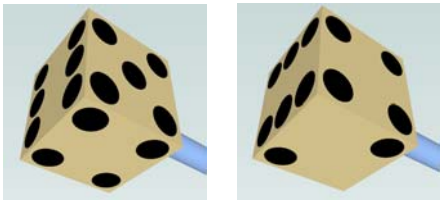

Fig. 2. A dice attached to a rod rotated (A) 0º and (B) 90º.

The second technique which was investigated involves changing the orientation of an object relative to a single vantage point. This was accomplished by rotating an object along an axis situated in an oblique orientation to the optical axis. Although this technique requires the specimen to be adjoined to a thin glass tip (and thus it is constrained to structurally integrated objects such as cells), it provides more z-axis information than the mirrored well, as the spacing between optical slices is only limited by the interval between rotations. This technique can also be coupled with MPWs by placing an object adjoined to a glass tip within a well, which may then be rotated around the stationary cell to generate five unique images per rotation angle per time point.

Cell Size and Cell Cycle Regulation

The use of reflection and rotation to obtain 3D data on biological specimens can be readily applied to the study of the size and shape of single cells. Because of the irregularities of cell shapes and the dynamics of cell growth, accurate measurements of cell size must be made in three dimensions. Existing techniques often do not provide measurements with enough precision to make conclusions about the process of individual cell growth, although the techniques described here may accomplish this task. A precise measurement of growing cell volume is important because of the insight it would give into the interaction between cell size and coupled intracellular phenomena which result in the maintenance of size homeostasis.

Cell growth and division are the result of a well-regulated sequence of biochemical events which are influenced by DNA content, protein concentration, cell size and the subcellular structure of individual cells. These processes are tightly coupled to cell cycle regulatory mechanisms, and an understanding of the intersection between regulatory signaling pathways and checkpoints and the maintenance of cell size homeostasis is important in descriptions of normal cellular processes, as well as diseased states, such as cancer, where control of cell cycle progression is lost as the inhibitions to continuous cell division are destroyed.

Budding yeast

One of the most important organisms in the investigation of cell cycle regulation is *Saccharomyces cerevisiae,* commonly known as budding yeast. *S. cerevisiae* is a simple, unicellular eukaryote which divides by an asymmetric budding process and is

widely used as a model organism. Mutational analysis of the budding yeast genome has allowed scientists to elucidate the subtle interactions between individual proteins involved in complex signaling pathways. These intracellular mechanisms are reflected in the size and structure of yeast cells, which give information both about the position of an individual cell within the cell cycle (chronological age) and the number of cellular divisions it has undergone (genealogical age). The major point of coordination between cell growth and division for budding yeast occurs at Start (labeled C_1 in Fig. 3), where cells commit to DNA replication and bud formation after reaching a critical size. The timing of C_1 relative to the cell growth rate determines the duration of the pre-Start growth phase (G_1), and in turn the average cell size of a population. The cell must also obtain a critical size to pass the pre-mitotic checkpoint (C_2) in order to initiate cell division. While the time of the G_1 phase depends on the genealogical age of the parent cell, the duration of growth prior to C_2 in G_2 phase is roughly the same for all cells (Hatzis and Porro 2006).

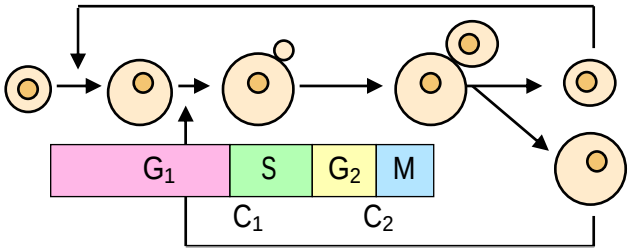

Fig. 3. Basic model of cell cycle progression of budding yeast (after Barberis *et al.* 2007).

Porro *et al.* (1995) determined that individual cell protein content increases exponentially during the cell cycle at the same rate for parent and daughter cells, but the exact nature of volume growth remains unknown. Early measurements on single cells found a roughly sigmoid volume increase, with the rate of growth slowing down at the end of G_1 phase prior to bud emergence (Hatzis and Porro 2006). Later, Hartwell and Unger (1977) found that the average rate of increase of the size of the mother before bud

emergence is less than the rate over the whole cycle. However, Woldringh *et al.* (1993) conducted a more thorough analysis in which they measured the cross sections of fluorescing cells and calculated the means of volume distributions of cells of various genealogical ages to argue for an exponential increase in volume.

Various mathematical models have been proposed to describe the growth phenomena of budding yeast populations. In one of the most recent efforts, Hatzis and Porro (2006) modeled the growth of a population of budding yeast by analyzing a system of temporally organized population balance equations which specify the physiological state vector based upon cell morphology. Following the conclusions of Woldringh *et al.* (1993), they assumed an exponential growth of individual cells throughout the cell cycle, although they state that concerns about experimental artifacts may question the validity of these results. The use of 2D data by Woldringh *et al.* also weakens their conclusion, as the assumption that cell shape is rotationally symmetric around an axis located in the xy plane is invalidated by observations of cells in the MPWs.

MATERIALS AND METHODS

Fabrication of Introverted Mirrored Pyramidal Wells

The mirrored pyramidal wells were fabricated by Ron Reiserer using anisotropic etching of silicon wafers in 40% KOH solution at 80 ºC. This process results in perfectly defined wells with molecularly smooth surfaces (Trupke *et al.* 2006). The etch angle was fixed at 35.3º to the normal, although the top and bottom dimensions and the depth can be controlled during etching. The wells used in this project had approximate top side lengths of 60 µm and bottom side lengths of 20 µm. The wells were then coated with aluminum to create mirrored surfaces on all five sides. Before using the mirrors, the part of the silicon wafer containing the etched mirrors was broken off from the rest of the wafer.

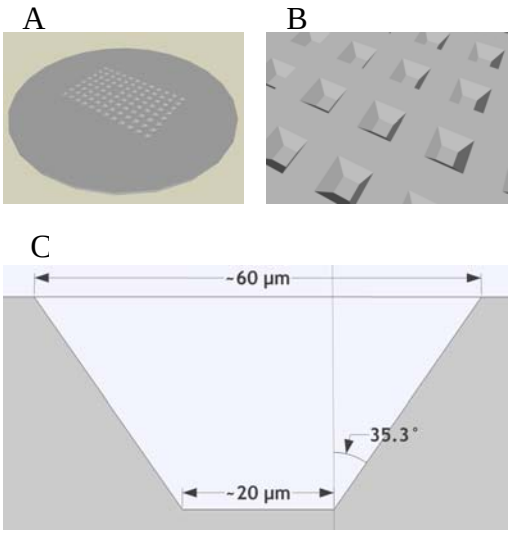

Fig. 4. Schematic of mirrored wells. (A) Etched silicon wafer. (B) Close-up view showing array of wells. (C) Geometry of the wells.

Microscope

All wide-field images were obtained using a Zeiss Axiotech Vario microscope (Fig. 5). Images were obtained using bright-field and fluorescence as detailed in the results. All images were captured with a Photometric CoolSNAP HQ digital camera using the SIDX (Bruxton) extension for ImageJ.

Fig. 5. Zeiss Axiotech Vario microscope.

Fluorescent Tip in Introverted MPWs

To test the introverted MPWs, images were collected of a fluorescent tip placed inside a well. I used a Narishige Microforge to melt the middle section of a glass capillary tube measuring 1 mm in diameter (Drummond Scientific) to create a small tip on the end of the tube. This was dipped in rhodamine and fluorescent images were obtained with a 5x air objective (NA 0.13).

Fluorescent Beads in Introverted MPWs

I gently pipetted fluorescent beads (Bang Lab) measuring 1 µm in diameter over the MPWs, which were submersed in a 50/50 solution of water and glycerol. Before the beads settled to the bottoms of the wells, images were obtained on a LSM510 META confocal microscope (Fig. 6).

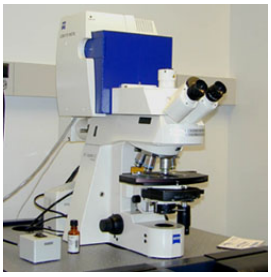

Fig. 6. LSM510 META confocal.

Yeast in Introverted MPWs

Small pellets containing dried *Saccharomyces cerevisiae* cells of strain K1-V1116 (Montepellier wine yeast) were used to start cultures. I mixed five to ten pellets with either a 1 mM solution of sucrose dissolved in tap water or yeast peptone dextrose (YPD) broth (Beckton-Dickinson), and the cells were allowed to incubate at room temperature at least 15 minutes before imaging. A small Petri dish (3 cm in diameter) was filled with 5 mm of either sugar water or YPD. The mirrors were gently placed on the bottom so as to remove any air bubbles, and 10-15 µL of the solution of growing yeast cells was pipetted

into the Petri dish. Images of the yeast cells were obtained with bright-field illumination with a 100x water immersion objective (NA 0.75).

I melted glass capillary tubes as detailed above to create tips for positioning the cells in the optimal center in the wells. Since the tips must be mounted parallel to the wafer in order to fit under the water immersion objective, I had to bend each end into a hook to fit it inside the MPWs. This was accomplished using a Narishige heating micromanipulator, which was also used to decrease the diameter of the tip to less than 5 µm (yeast cells used in the experiments were typically 8-10 µm in diameter). In order to position cells on the very end of the pulled tips, Cell-Tak (Becton-Dickinson), a formulation of polyphenolic proteins extracted from *Mytilus edulis* (marine mussel), was used. 10 µL was pipetted onto a glass slide, followed by a drop of ethanol. This was exposed to room conditions for 3 minutes, then a glass tip was pulled through the drying solution several times. This tip was immediately used. The pulled glass tip was held in place by a pin vise attached to a micromanipulator (Eppendorf), which was used to position the tip in the x-, y- and z-directions as desired.

Rotating Introverted MPWs

Two manual translating mechanical style slides (Thor Labs) were stacked with their directions of motion perpendicular, and a manual rotating slide (Newport) was then placed on top of them, followed by two more translating slides. A Petri dish containing the mirrored wells was placed on top of this setup, and a single well was positioned near the axis of rotation by the top pair of translating slides and in the center of the field of

view by the bottom translating slides. The rotating slide could then be manually cycled through a set angle.

Fabrication of Extroverted MPWs

Mirrored pyramidal wells whose object location is outside the well, termed extroverted MPWs, were to be created by stamping a hexagonal tip into a polished plate of softer aluminum. Steel and tungsten carbide were used as the materials for the stamp. I first polished the tip of the stamp using a Dremel hand grinder/polisher, then polished the tip to contain six slanted hexagonal faces and a flat end using a holder machined by Dr. Seale, which allowed rotation of each tip through 60º per polishing step. The tips were polished on a Metaserv 2000 (Buehler) grinder/polisher using a polishing cloth and a diamond grit surface (Buehler) for the steel and tungsten carbide stampers, respectively. Each was polished using first a 50 nm then a 20 nm non-crystallizing colloidal silica polishing suspension (Buehler). Before and after polishing the stamps with these suspensions, I gently polished the tips with just water. Before examining the results under the light microscope to check for a hexagonal geometry, the polished tips were sonicated using a Cole-Parmer ultrasonic cleanser (Model 8891) to remove debris from the polishing process. The results of the polishing process were imaged with a Hitachi S-4200 Scanning Electron Microscope (SEM) to examine the polished surface for imperfections not visible under the light microscope (Fig. 7).

Fig. 7. Hitachi S-4200 SEM.

Rotating Tomography

A stepper motor was connected to a unipolar stepper motor driver (Modern Technology). The driver was connected to a computer through a parallel-port connection to gain control of the rotation. A pin vise was placed onto the end of the stepper motor, along the axis of rotation. A glass capillary 2 mm in diameter with a straight tapered end made with the Narishige heater was placed into the pin vise. To test this setup, a piece of Orbit chewing gum measuring 1 mm in diameter was placed on the end of the tip, and the motor was manually cycled through a full rotation at 10º intervals (Fig. 8). Images were obtained using a 5x air objective (NA 0.13) under bright-field illumination.

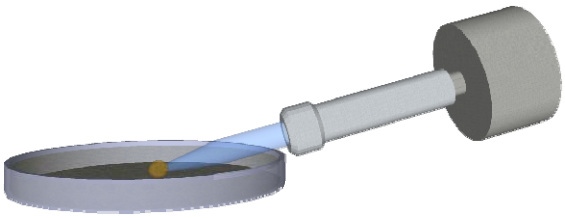

Fig. 8. Setup of rotation experiment. The pulled glass tip to which the object to be rotated is adjoined is held inside a pin vise secured to the axis of rotation of a stepper motor.

RESULTS AND DISCUSSION

Introverted Mirrored Pyramidal Wells

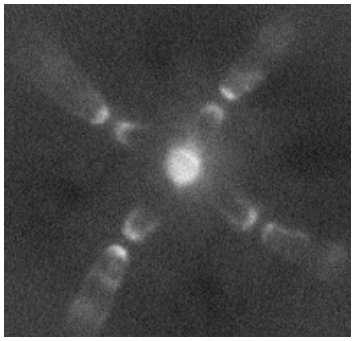

Fig. 9. Fluorescent tip in a MPW. Five primary and four secondary reflections are visible.

Mirrored pyramidal wells provide up to five nearly orthogonal views of a specimen. When a pulled glass tip dipped in rhodamine is placed equidistant from each mirrored surface (in what is termed the optical center of the MPW) and viewed with fluorescent illumination, nine reflected images are formed in a single focal plane (Fig. 9). Four primary reflections from each of the angled sides are visible, as well as four secondary reflections given by the reflection of these virtual images off the bottom of the well. In general, these secondary reflections are not visible where contrast is much lower (i.e., where no fluorescence is involved). The primary reflection from the bottom of the well appears as a bright spot near the center. It is more intense than the other reflections because the tip is located close enough to the bottom that light from the real image is collected in the same focal plane. Because this reflection provides no information which is not already contained in the real image, the distinction between these two images is less important than for those available from the angled sides. However, the reflection from the bottom surface can still be distinguished from the real image when the object is located a sufficient distance above the bottom of the well.

The mirrored wells represent a theoretical five-fold increase in the collection efficiency of the microscope since a greater portion of the solid angle is redirected into the objective. However, the signal intensity of the mirror images is less than the real

A

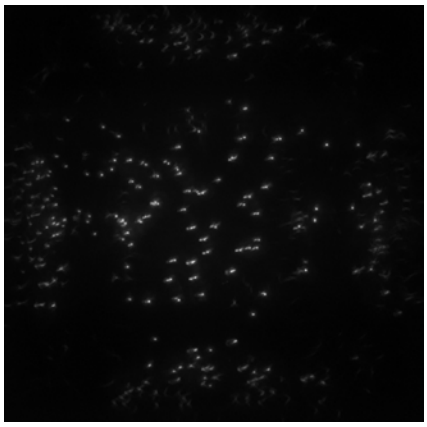

B

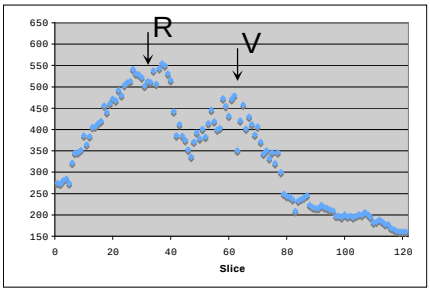

Fig. 10. Multiple fluorescent beads in a MPW. (A) Max intensity Z-projection. (B) Z-axis profile.

images. 1 µm diameter fluorescent beads were suspended in a 50/50 solution of water and glycerol and an image stack was obtained using a confocal microscope, as illustrated in Fig. 10. (A) shows the maximum intensity Z-projection from each image in the stack, which clearly shows the position of the beads and their reflections formed from the four angled sides, which appear less bright than the real images of the beads. (B) shows the maximum intensity Z-axis profile. The maximum intensity value of slices corresponding to the virtual object (V) is approximately 90% of the value of images of the real object (R). This loss is expected, as aluminum reflective coatings give an average reflectance of 90% over the visible spectrum ("Optical Coatings"). Despite this decrease in the intensity, the images collected of the reflections still represent a significant increase in total light collected from the specimen and in the information content of each image.

Dr. Kevin Seale previously obtained images of a pollen grain from a *Helianthus annuus* (sunflower) anther and a *Dictyostelium discoidum* amoeba, demonstrating that the mirrors can faithfully reproduce the fine features of a specimen without aberrations. In order to investigate image formation under conditions of high magnification, *S. cerevisiae* cells in the MPWs were examined using a 100X objective (NA 0.75). The image in Fig. 11 was obtained from a single cell in sugar water. The cell shown in (A),

which is not located in the center of the well, casts reflections which are visible at different focal depths, as illustrated in (B). The change in position of the cell between these two images, visible by comparing the cell in (A) and the reflection off the bottom surface in (B), should also be noted. The binary images shown in (C) and (D) were obtained using an edge-detection plug-in for ImageJ. Cell perimeters were found for three of the four reflections, and fine internal structures, such as what appears to be the vacuole in the middle of the cell, are visible both in the real images and in the reflections. One method for obtaining more accurate perimeters for each image is to use fluorescence, thus eliminating background illumination (compare the contrast between the specimen and the MPW in Figs. 9 and 11).

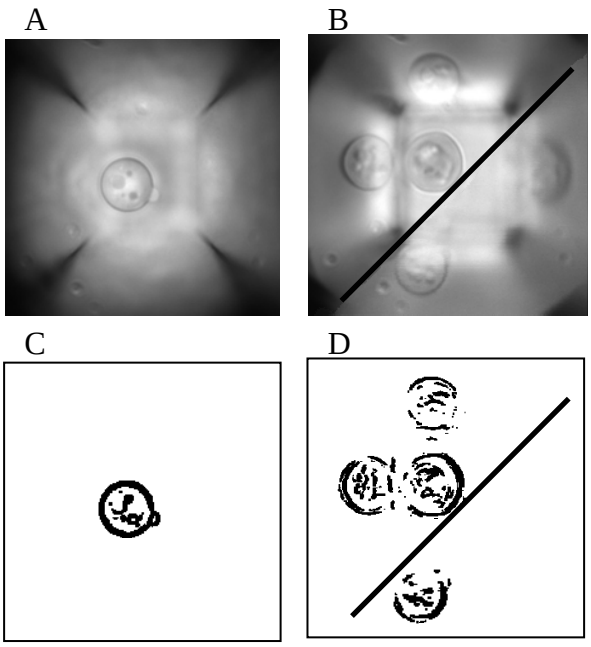

Fig. 11. A single yeast cell in a MPW. (A) Real image of the cell. (B) Reflections of the cell at different focal planes. (C-D) Corresponding binary images.

The first biological measurement which will be made with the MPWs is the volume of a growing yeast cell as it passes through the cell cycle. This measurement is important because of the information it can yield about the connection between growth and cell cycle regulatory mechanisms. It is also a good first step for testing the ability of the mirrors to generate images which can be used to reconstruct an accurate 3D model because of the simple shape of the yeast cells. In order to measure the cell size at a given time point, a back-projection algorithm must be used to reconstruct a 3D model from

binary images such as those shown in Figs. 11 and 12, in which the perimeter of the cells can be easily defined. At each time point, this data will then be fit to a simple 3D model to generate a surface which can be integrated to give the volume. For this purpose the spherical harmonics, which can faithfully reproduce 3D features of objects (Matheny and Goldgof 1995) will be used.

One complication arises from the fact that *S. cerevisiae* cells reproduce through a budding process, as shown in Fig. 12. In this image, the yeast cell is near the optical center, and the reflections from three of the angled sides as well as the bottom surface are found in the same focal plane. In reflections from the north and south sides, the mother cell occludes the daughter cell so that information about its shape is only available from the east and west reflections. This presents a difficulty both for determining the boundaries between cells and for formulating an accurate 3D description of the cells' shape. But even if the shape of the yeast cell as determined by its reflections is less constrained than in other cases, the additional images still represent an improvement over the measurements of Woldringh *et al.* (1993), which only looked at 2D images equivalent to those shown in (A) and (C) when analyzing yeast cell size

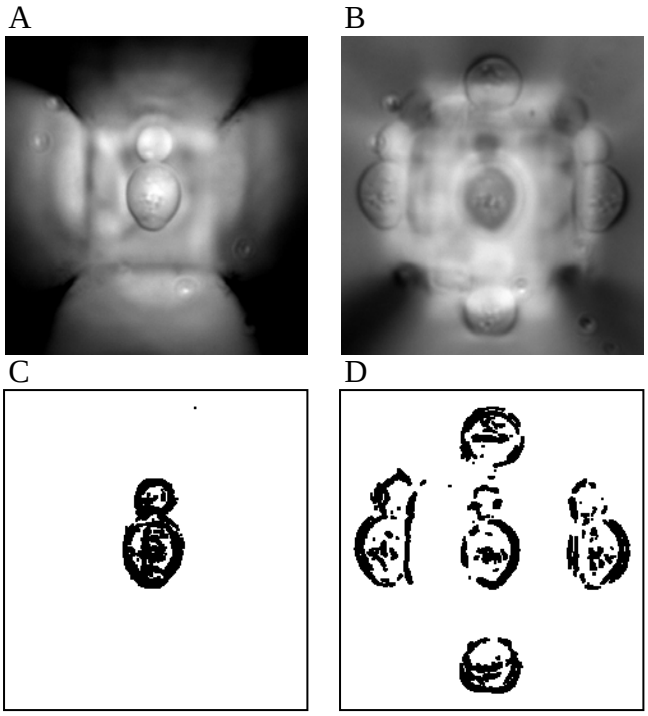

Fig. 12. A budding yeast cell in a MPW. (A) Real image of the cell. (B) Reflections of the cell in one focal plane. (C-D) Corresponding binary images.

growth. None of the yeast cells shown above fit the assumption used by Woldringh *et al.* that the cells are perfect spheroids (that is, that an image in one plane can be rotated about the center of the cell to faithfully reproduce shape in 3D).

Information about an object placed within a MPW can be obtained from a maximum of five vantage points. However, additional data for each time point may be necessary to reconstruct cellular shape in 3D with the required precision. This can be achieved by including rotation as a source of additional viewpoints. An object can be positioned in the optical center of a well using a glass tip. The wells, which are placed in the center of a rotating slide, are then allowed to rotate through fixed increments around the object (Fig. 13). This generates five unique views for each rotation angle. If the object is rotated through 10º increments, this results in forty-five near-simultaneous distinct images.

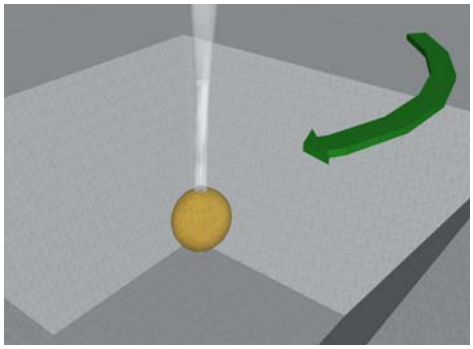

Fig. 13. Schematic of a MPW rotating about an object adjoined to a glass tip.

Images of a yeast cell placed within a well by a pulled glass tip are shown in Fig. 14. The cell can easily be positioned in the optical center of the well, but the glass obscures two of the four reflections almost completely because the cell is located on the side of the tip. This could be remedied by ensuring that the cell is on the very end of the glass. Because all of our efforts to attach the cell to the tip by contact alone resulted

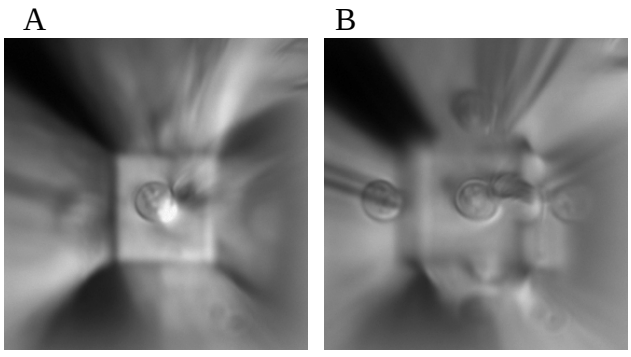

Fig. 14 A yeast cell on a glass tip in a mirrored well with (A) the real image and (B) reflections.

in the cell resting on the side of the tip, an adhesive such as Cell-Tak might be used to ensure that once the cell comes into contact with the end of the tip, it will remain in the desired position (data not shown).

In order to accurately reconstruct the 3D shape of an object, the geometry of the well and the exact position of the object within the well must be known. The former is easily determined by measuring the top and bottom side lengths. The latter is more difficult when considering reflections taken at different focal depths (which occur when the object is not located in the optical center of the well). However, rapid optical sectioning through the well with a z-stack can provide the necessary information to construct an accurate 3D model by giving the position of the focal planes in which the images are found relative to the known dimensions of the well. Figs. 11 and 12 demonstrate the ability of the MPWs to provide simultaneous information from five nearly orthogonal viewpoints, and rapid z-sectioning will provide a way to interpret this data in 3D so that the dynamics of cell size growth of budding yeast can be quantified.

Extroverted Mirrored Pyramidal Wells

Extroverted mirrored pyramidal wells, whose optical center would be located outside the wells, can also be envisioned. These MPWs could be placed above an object, thus allowing imaging of cells located on a variety of substrates. An extroverted MPW can be made by embossing the mirrors into a piece of aluminum, leaving behind

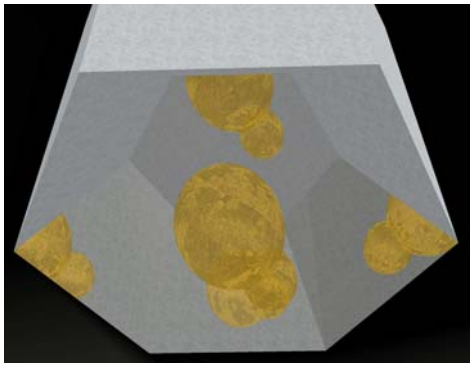

Fig. 15. Schematic of an extroverted MPW positioned above a budding yeast cell.

an indentation with six angled sides and one flat side, as diagrammed in Fig. 15. Stainless steel rods were first used as the stamping material, but they created mirror surfaces with aberrations which prevented accurate image formation. After stamping one mirror, the stainless steel also became deformed and could not be used to manufacture additional mirrors. One alternative is tungsten carbide, which is much harder than stainless steel. However, its toughness also makes this substance more difficult to work with. After polishing the tungsten carbide embosser into a roughly hexagonal shape, I took electron micrographs of the surface of the rod (Fig. 16). They demonstrate surface imperfections, most likely as a result of the polishing process, which would result in the fabrication of imperfect mirrors. Before extroverted MPWs can be implemented, we must overcome the problem of creating a durable embosser which has surfaces that are flat to within the required precision. Because intermediate polishing steps are important for the creation of smoother surfaces, the polishing process will be repeated using colloidal silica polishing suspensions of size intermediate between 50 nm and 20 nm, which were used to polish the surface shown in Fig. 16. In addition, replica coating and aluminization can be used to give a smoother surface.

A

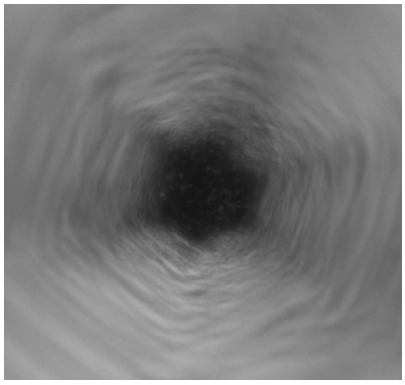

B

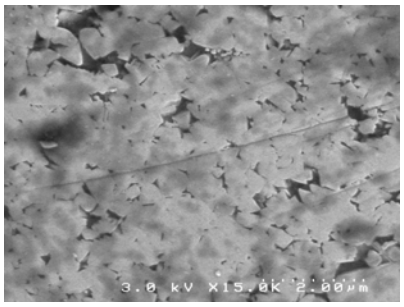

Fig. 16. Tungsten carbide impresser. (A) Bright-field image, 20x objective. (B) Electron micrograph.

Rotating Tomography

Bray *et al.* (2000, 2002) used a system of two mirrors combined with rotation of a rabbit heart to obtain 3D information about its shape, which they constructed using the method of occluding contours as discussed in Niem (1994). This technique slices out the silhouette formed by an object, and through the use of multiple vantage points one can slice out a convex hull which approximates the object's shape very well (if there are no concavities). The technique of generating multiple viewpoints by rotation was extended to microscopy by implementing the setup shown in Fig. 8. To test the validity of this approach, a small piece of chewing gum measuring about 1 mm in diameter was imaged at 5x in air, rotating through 360º at 10º intervals. The resulting images were thresholded to create a stack of binary images showing the outline of the gum (Fig. 17). If each of these images was assumed to describe an object symmetric about rotation through the y-axis according to the protocol of Woldringh *et al.* (1993), the average of the volume found for each slice could be used to obtain an estimate of the volume. However, a reconstructed 3D object more accurately describes the volume because it does not involve assumptions about the shape of the object, and it represents a coherent 3D body, instead of an average over a finite number of frames.

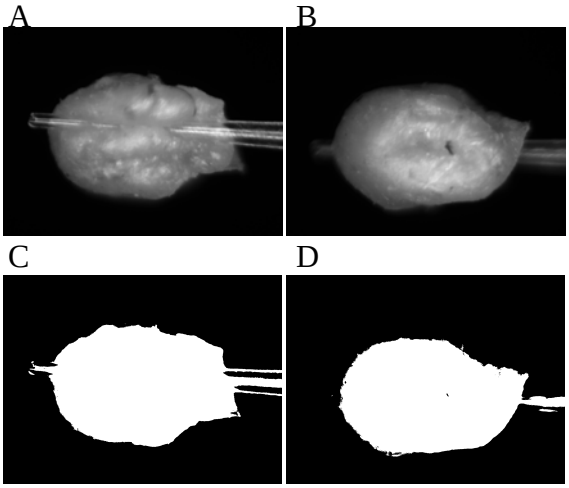

Fig. 17. Images of the gum on a tip after (A) 0º and (B) 180º of rotation and corresponding binary images (C-D).

This stack was then analyzed using an algorithm which follows the procedure outlined by Bray *et al.* (2000). In Matlab, a cube of data points which could encompass the entire object was created, and each image was read sequentially from the stack. An array in the middle xy plane of the cube was compared to the first binary image, and xy points which fell outside this volume were set to zero for all values of z for the cube. This corresponds to shaving out the outline of the image from one viewpoint. Then the cube, which represents the final 3D object, was rotated through the same angle as the gum to shave off more points corresponding to the area outside the next slice. This process was repeated for each image through 360º of rotation.

Bray *et al.* (2000) used a perspective projection matrix to determine the depth of the data points from their 2D image in order to obtain an accurate reconstruction. However, this is not necessary for images obtained through a microscope, where the image plane is located a sufficient distance from the object to justify the assumption of the limit of weak perspective. One complicating factor which cannot be ignored in the microscopic setup is that the object does not simply rotate on an axis, but also around it (compare panels A and B in Fig. 17). This is because the capillary tube is not completely fixed into place, and due to the small size of the object variations in the movement of the capillary tube must be included in the analysis. This was implemented

A

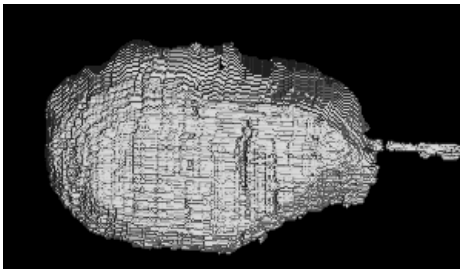

B

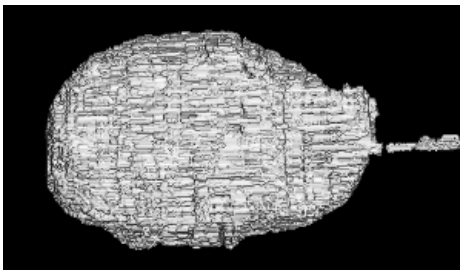

Fig. 18. Snapshots of the reconstructed 3D object corresponding to (A) 0º and (B) 180º of rotation.

by ensuring that the end of the glass tip was always located at the origin before applying the rotation matrices. The tip was first rotated about the z-axis to align it with the y-axis, then rotated 10º about the y-axis, and finally rotated back along the z-axis before being translated back to its original position to implement the occluding contours routine. Snapshots of the reconstructed object are shown in Fig. 18. A movie showing rotation of the reconstructed object through a full 360º is included in supplemental materials.

Only images 25% of the size of the original images have been analyzed due to the computational costs of the occluding contours algorithm. Kay *et al.* (2004) improved upon the method of Bray *et al.* (2000) by incorporating an adaptive octree mesh refinement algorithm, which Qu *et al.* (2006) later refined. This algorithm sections the sample into octants which are examined for the presence of edges. If any octant contains an edge, it is further subdivided until the desired resolution is reached, at which point the contours are shaved out. By implementing octree refinement in the current algorithm, larger data sets could be handled. Brodland and Velduis (1998) collected macroscope images of a rotating *Ambystoma mexicanum* (axolotl) embryo, which they analyzed by block analysis to establish point correspondences between different images and accommodate for camera positioning errors. The application of this method to microscope images will also be investigated so that we can implement a more sophisticated reconstruction technique involving both occluding contours and block matching.

One advantage of the technique of rotating tomography over the mirrored wells is that it does not require a z-stack to obtain interpretable data. Its provides more data than can be gathered from a cell sitting inside a stationary well, and the data is easier to

analyze because there is little light pollution (as opposed to reflections off the sides of the well) which would otherwise render the simple application of an edge detection algorithm much more difficult. This would make studies of the 3D dynamics of subcellular objects easier, as an edge-detection algorithm could be implemented to allow for multiple threshold levels corresponding to the outline of the cell and of the desired subcellular object. This would provide a 3D reconstruction of the object of interest and its 3D location within the cell.

Questions may arise about perturbations to the growth of the cell created from adhering it to the surface of the tip, so comparisons of volume measurements made with both MPWs and rotation will be useful to corroborate the data. In addition, accurate data gathering and long time scale measurements require complete computer control of the system. The use of yeast cells in this system is also complicated by the fact that the size of the yeast cell is much smaller than that of the gum with respect to the motion of the tip, so the microscope must be refocused and the cell repositioned in the field of view each time it is rotated. However, the occluding contours algorithm could still be applied to the cell by first calibrating the setup by rotating it at a lower magnification. Because the end of the tip describes a circle rotated in 3D, measurements of its position at each point can be used to reconstructed the orientation of the axis about which the tip is rotating (data not shown). This information could be used to calibrate a z-stack to refocus to the correct depth and computer control of the micromanipulator to maintain the cell in the center of the field of view. Adjustment screws may also be added to the pin vise to confine the limit the extent of the off-axis rotation of the tip.

CONCLUSIONS

Two methods for obtaining 3D data of biological specimens were examined. The introverted mirrored pyramidal wells were shown to produce high resolution images of yeast cells from multiple vantage points. By coupling this system with a z-stack, images will be taken of a budding yeast cell as it progress through the cell cycle in order to measure changes in its cell size. This system may also be readily integrated into a microfluidics by placing the cell traps at the top edges of the introverted MPWs so that 3D data about cells in the traps may be determined. This will prove useful in determining rapid morphological changes in response to varying environmental conditions. More precise measurements on cells in the introverted MPWs can also be made by rotating the wells around a stationary cell to obtain a more complete tomography, and measurements using this technique can be carried out once more control is gained over the rotation of the wells. Another use of MPWs is through extroverted wells, which can be placed above the specimen, thus obviating the need for it to sit within a well. This can also be implemented and coupled with microfluidics once a more reliable manufacturing process is worked out.

Finally, the use of rotation to make 3D measurements upon single cells was investigated. By rotating a piece of chewing gum about 360º, a close approximation to its true shape can be reconstructed using an occluding contours algorithm. Once computer control of the micromanipulator is established in order to ensure consistent experimental conditions, this algorithm can be applied with minor adjustments to reconstruct the shape of a growing cell attached to a glass tip which is rotated at every time step. Together with

the MPWs, this presents a new way to obtain accurate z-information which can be used with conventional wide-field microscopy, and which addresses some of the problems with z-resolution faced by other 3D microscopy techniques by obtaining near-orthogonal images slices.

ACKNOWLEDGMENTS

This research has been supported by the Vanderbilt Institute for Integrative Biosystems Research and Education, the Systems Biology and Bioengineering Undergraduate Research Experience, and the William and Nancy McMinn Honor Scholarship in Natural Science. Thank you to Kevin Seale, who taught me many of the techniques and provided significant intellectual support, and to Ron Reiserer, who made the introverted MPWs and put together the rotation setup. Thank you also to John Wikswo for providing many ideas for improvement of the techniques and for acting as faculty advisor. I appreciate the encouragement of Erik Boczko. I would also like to thank Shane Hutson, Chris Janetopoulos and David Weintraub for serving on the committee of independent examiners for this work.

REFERENCES

Amos WB and White JG. How the confocal laser scanning microscope entered biological research. *Biol Cell* **95**, 335-342 (2003).

Barberis M, Klipp E, Vanoni M and Alberghina L. Cell size at S phase initiation: an emergent property of the G1/S network. *Comp Biol* **3**, 649-666 (2007).

Bray MA, Lin SF and Wikswo JP. Three-dimensional surface reconstruction and fluorescent visualization of cardiac activation. *IEEE T Biomed Eng* **47**, 1382-1391 (2000).

Bray MA, Lin SF and Wikswo JP. Three-dimensional visualization of phase singularities on the isolated rabbit heart. *J Cardiovasc Elect* **13**, 1311-1312 (2002).

Brodland GW and Veldhuis JH. Three-dimensional reconstruction of live embryos using robotic macroscopic images. *IEEE T Biomed Eng* **45**, 1173-1180 (1998).

Conchello JA and Lichtman JW. Optical sectioning microscopy. *Nat Meth* **2**, 920-931 (2005).

Denk W, Strickler JH and Webb WW. Two-photon laser scanning fluorescence microscopy. *Science* **248**, 73-76 (1990).

Harold FM. Force and compliance: rethinking morphogenesis in walled cells. *Fungal Genet Biol* **37**, 271-283 (2002).

Hartwell LH and Unger MW. Unequal division in Saccharomyces cerevisiae and its implications for the control of cell division. *J Cell Biol* **75**, 422-435 (1977).

Hatzis C and Porro D. Morphologically-structured models of growing budding yeast populations. *J Biotech* **124,** 423-438 (2006).

Kay MW, Amison PM and Rogers JM. Three-dimensional surface reconstruction and panoramic optical mapping of large hearts. *IEEE Trans Biomed Eng* **51** (2004).

Matheny A and Dmitry B. The use of three- and four-dimensional surface harmonics for rigid and nonrigid shape recovery and representation. *IEEE T Pattern Anal* **17**, 967-981 (1995).

McNally JG, Karpova T, Cooper J and Conchello JA. Three-dimensional imaging by deconvolution microscopy. *Method* **19**, 373-385 (1999).

Niem W. Robust and fast modelling of 3D natural objects from multiple views. *SPIE P-Image Video Process II* (1994).

"Optical Coatings". *Optics Guide*. Melles Griot, Inc. Updated 2002. < http://www.mellesgriot.com/products/optics/oc_5_1.htm>.

Porro D, Ranzi BM, Smeraldi C, Martegani E and Alberghina L. A double flow cytometric tag allows tracking of the dynamics of cell cycle progression of newborn Saccharomyces cerevisiae cells during balanced exponential growth. *Yeast* **11**, 1157-1169 (1995).

Prasad V, Semwogerere D and Weeks ER. Confocal microscopy of colloids. *J Phys Condens Matt* **19**, 113102 (2007).

Qu F, Ripplinger CM, Nikolski VP, Grimm C and Efimov IR. Three-dimensional panoramic imaging of cardiac arrhythmias in rabbit heart. *J Biomed Opt* **12** (2007).

Rueden CT and Eliceiri KW. Visualization approaches for multidimensional biological image data. *Biotechniques* **43**, 31-36 (2007).

Seale KT, Reiserer RS, Markov DA, Ges IA, Wright C, Janetopoulos C and Wikswo JP. Mirrored pyramidal wells for simultaneous multiple vantage point microscopy (2008). Manuscript submitted for publication.

Shaw PJ, Agard DA, Hiraoka Y and Sedat JW. Tilted view reconstruction in optical microscopy. Three-dimensional reconstruction of Drosophila melanogaster embryo nuclei. *Biophys J* **55**, 101-110 (1989).

Trupke M, Ramirez-Martinez F, Curtis EA, Ashmore JP, Eriksson S, Hinds EA, Moktadir Z, Gollasch C, Kraft M, Vijaya Prakash G and Baumberg JJ. Pyramidal micromirrors for microsystems and atom chips. *App Phys Lett* **88** (2006).

Woldringh CL, Huls PG and Vischer NO. Volume growth of daughter and parent cells during the cell cycle of Saccharomyces cerevisiae a/alpha as determined by image cytometry. *J Bacteriol* **175**, 3174-3181 (1993).

Ziegler, U, Bittermann AG and Hoechli M. "Introduction to Confocal Laser Scanning Microscopy". University of Zürich. <http://www.zmb.uzh.ch/resources/download/CLSM.pdf>.

APPENDIX A

Matlab code to implement occluding contours algorithm

Reconstructs an object in 3D from its silhouettes
Program author: Charlie Wright
Created: 10 April 2008
Last modified: 17 April 2008

```
clear all; clc

fileName = input('Enter file name: ','s');
scale = input('Amount images scaled from original: ');
fileInfo = imfinfo(fileName);

% Find the number of images in the stack
fileInfoSize = size(fileInfo);
frameMax = fileInfoSize(2);

% Find the dimensions of each image (should be the same for all images)
rMax = fileInfo(1).Height;
cMax = fileInfo(1).Width;
zMax = rMax; zHalf = ceil(zMax/2);

% Make 3D array of ones from which to carve out contours
cont = ones(rMax,cMax,zMax);

% Movement of tip measured in ImageJ (differs for each stack)
xTip = [458 436 402 393 381 378 372 377 385 392 406 432 466 510 537 560 582 605,...
    628 644 678 704 714 720 722 716 702 725 681 637 612 590 544 518 476 457].*scale;
yTip = [129 137 136 134 138 136 142 152 149 152 150 152 152 154 157 152 156 150,...
    148 145 137 137 137 137 132 126 125 120 121 116 120 117 120 124 128 129].*scale;
alpha = -[-3.629 -3.745 -3.925 -3.967 -4.049 -3.959 -3.869 -3.722 -3.594,...
    -3.378 -3.18 -3.004 -2.644 -2.18 -1.971 -1.849 -1.735 -1.423 -1.347,...
    -1.045 -0.881 -0.684 -0.841 -0.612 -0.649 -0.763 -1.106 -1.223 -1.453,...
    -2.106 -2.364 -2.49 -2.999 -3.161 -3.426 -3.538].*pi/180;

for frame = 1:frameMax

    % Read image and convert to binary
    slices = zeros(rMax,cMax,zMax);
    slices(:,:,zHalf) = im2bw(imread(fileName,frame),0.5);

    if frame == 1

        % Translation to origin
        TM1 = eye(4);
        TM1(4,1) = -xTip(1); TM1(4,2) = -yTip(1); TM1(4,3) = -zHalf;

        RM = [cos(alpha(frame)) -sin(alpha(frame)) 0;
              sin(alpha(frame))  cos(alpha(frame)) 0;
              0                  0                 1];
        RM = vertcat(horzcat(RM,zeros(3,1)),zeros(1,4)); RM(4,4)=1;

        % Translation to location of tip
        TM2 = eye(4);
        TM2(4,1) = xTip(1); TM2(4,2) = yTip(1); TM2(4,3) = zHalf;

    else

        % Translation to origin
        TM1 = eye(4);
        TM1(4,1) = -xTip(frame-1); TM1(4,2) = -yTip(frame-1); TM1(4,3) = -zHalf;

        % Rotation along y-axis
        phi = pi/18;            % Rotation angle of shaft
        phiRM = [ cos(phi)  0   sin(phi) ;
                  0         1   0        ;
```

```
                -sin(phi)  0   cos(phi) ];
        alphaRM1 = [cos(alpha(frame-1)) -sin(alpha(frame-1)) 0;
                    sin(alpha(frame-1))  cos(alpha(frame-1)) 0;
                    0                    0                   1];
        alphaRM2 = [cos(alpha(frame)) -sin(alpha(frame)) 0;
                    sin(alpha(frame))  cos(alpha(frame)) 0;
                    0                  0                 1];

        RM = alphaRM1'*phiRM*alphaRM2;
        RM = vertcat(horzcat(RM,zeros(3,1)),zeros(1,4)); RM(4,4)=1;

        % Translation to location of tip
        TM2 = eye(4);
        TM2(4,1) = xTip(frame); TM2(4,2) = yTip(frame); TM2(4,3) = zHalf;

    end

    % Apply affine transformation
    T = maketform('affine',TM1*RM*TM2);
    R = makeresampler('nearest','fill');
    cont = tformarray(cont,T,R,[1 2 3],[1 2 3],size(cont),[],0);

% Set entries in cont which do not intersect slices to 0
    for r = 1:rMax
        for c = 1:cMax
            if ~slices(r,c,zHalf)
                cont(r,c,:) = 0;
            end
        end
    end
end

name = ['cont2-',num2str(scale),'.tif'];
for z = 1:zMax
   imwrite(cont(:,:,z),...
       ['C:\Documents and Settings\Administrator\My Documents\MATLAB\PHYS296\',name],...
       'tiff','Compression','none', 'WriteMode','append');
end
```

APPENDIX B

Mirrored Pyramidal Wells for Simultaneous Multiple Vantage Point Microscopy

Kevin T. Seale, Ronald S. Reiserer, Dmitry A. Markov, Igor A. Ges, Charles Wright, Chris Janetopoulos, and John P. Wikswo[†]

ABSTRACT

We report a novel method for obtaining simultaneous images from multiple vantage points of a microscopic specimen using size-matched microscopic mirrors created from anisotropically etched silicon. The resulting pyramidal wells enable bright field and fluorescent side-view images, and when combined with z-sectioning, provide added information for three dimensional reconstructions of the specimen. The simultaneous acquisition of multiple perspectives also provides a five-fold increase in the theoretical collection efficiency of emitted photons.

INTRODUCTION

Microscopy is normally conducted within a single focal plane (XY) at a specific axial depth (Z) providing a single two dimensional (2D) image or stack of images. Since biological systems are highly dynamic and often undergo coordinated inter and

[†]Contact: john.wikswo@vanderbilt.edu
Professor of Biomedical Engineering, Molecular Physiology & Biophysics, and Physics
Vanderbilt University
VU Station B 351807 (U.S. Postal Service)
Nashville, TN 37235-1807 USA
6301 Stevenson Center (UPS and Fedex)
Nashville, TN 37232 USA
Phone: (615) 343-4124 Fax: (615) 322-4977 ...

intracellular motion in all three spatial dimensions, it becomes very difficult to capture these movements with standard wide-field or confocal microscopy. We have explored the use of cell-sized mirrors formed by the angled sidewalls of anisotropically etched pyramidal wells in silicon for conducting microscopy from multiple vantage points (**Fig 1A**). The mirrored pyramidal wells (MPW) provide multiple, nearly orthogonal views of the specimen, increase the collection efficiency of the imaging system and are compatible with biomicroelectromechanical (bioMEMS) devices. The MPWs are fabricated using anisotropic etching of silicon wafers in 40% KOH solution at 80 C which results in perfectly defined wells with molecularly smooth surfaces(Trupke *et al*). The etch angle is fixed at 54.7º and the dimensions of the top, bottom and depth can be sculpted as desired. They are then coated with either platinum, aluminum or other metals to provide up to five simultaneous views of the specimen from nearly orthogonal vantage points (**Fig 1B-E**), a high magnification side-view image from a single mirror (**Fig 1F**), or six views using a z-stack and imaging the reflection off the bottom of the well (not shown).

Another advantage offered by MPW microscopy over other mirror and side-view microscopy methods(Leyton-Mange *et al*; Bell and Jeon; Gustaffson and Wolpert; Boocock *et al*; Cao *et al*; Dong *et al*;Harris; Hlinka and Sanders; Roth *et al*; Sanders and Prasad) is the ability to fabricate controlled sizes of the mirrored wells. Standard photolithography methods enable feature sizes as small as 2 microns and as large as several hundred microns, allowing MPWs to be custom-sized for a particular specimen. MPWs enable interrogation with short working-distance objectives that are physically obstructed by larger mirror systems(Sheppard; Stelzer and Lindek). When a 25 μm glass pipette is placed at the optical center of the MPW, five reflected images are formed in a

single, reflected focal plane (**Fig 1 D,E).** The central, reflected image in **1D** is less intense due to obstruction of the collection cone by the real object, while it is more intense in **1E** possibly due to more efficient fluorescence excitation. The mirrors (**Fig 1A**) can faithfully reproduce the fine features of a specimen without aberrations. **Figure 1C** illustrates the fine, spiky projections of a *Helianthus annuus* pollen grain in profile from four sides (see Supplementary **Figs 1C**); had the grain been elevated in a slightly larger well, the central image would have been in focus with the other four. At higher numerical apertures consideration must be given to the possibility of mismatch between the angles of the collection cone and the MPW wall. However, high magnification image formation is possible as illustrated in a reflected bright field five way image of a single *Sacchromyces cerevisiae* cell using a 100X objective (NA 0.75) in an MPW (**Fig 1F** and Supplementary movie **1F**). The five images shown in **Fig 1E** illustrate a theoretical 5-fold increase in the collection efficiency of MPW microscopy over conventional means since a greater portion of the total available solid angle (4π steradians) is redirected into the objective. This equates to an increase in detection sensitivity and higher signal-to-noise ratios for imaging fluorescent or luminescent samples.

Three dimensional microscopy with MPWs offers advantages over other methods because the mirrors reorient the point spread function (PSF) of the objective. The PSF is the complex 3D intensity pattern resulting from a point source of light near the focal plane of a microscope. The accuracy of three dimensional (3D) microscopy is ultimately limited by the PSF, which is roughly hour-glass shaped and is ordinarily axially elongated and symmetric about the image plane of the microscope(Abbe; Born M. and Wolf E.). The shape of the PSF and the location of its minima determine the in-plane

resolution limit (approximately 200 nm) as well as the axial resolution of 3D imaging by optical sectioning microscopy (OSM)(Strutt JW (Lord Rayleigh)). Each OSM "slice" arises from a finite slab of the specimen and contains out of focus light from adjacent slices. The 3D-PSF must be deconvolved from the OSM image stacks to recover the more true 3D structure of the specimen. Iterative, constrained deconvolution is an excellent way to interpolate the missing axial information, but requires time for acquisition and implementation(Agard and Sedat). Tilted view microscopy (TVM) reorients fixed samples relative to the optical axis, acquiring different cross-sectional images with high in-plane resolution that are recombined into a 3D model(Shaw *et al*;Shaw; Bradl *et al*). TVM is limited by precise alignment requirements and the necessity for fixed specimen. Other methods for very high resolution imaging such as theta, 4Pi, and I^5M all share the common feature of collecting more light from more directions around the sample by multiple objectives or macro-sized mirrors(Cogswell *et al*; Gustafsson *et al*; Hell *et al*; Hell and Stelzer; Lindek *et al*; Lindek *et al*; Stelzer and Lindek). MPWs offer an exciting and unprecedented opportunity to obtain fast and accurate 3D information of live specimen from several nearly-orthogonal directions simultaneously. **Figure 2** illustrates the orientation and location of the multiple single-reflection tilted views of a sample specimen denoted $\beta,\gamma,\delta,\varepsilon$ and ϕ as well as secondary and tertiary reflections (not shown). The figure shows that all six faces of the die are visible, and at any die orientation five of the six faces will be simultaneously visible in the reflections, and the sixth can be observed directly with no reflection at a different focal depth.

Biology exists and functions in all three spatial dimensions simultaneously, and dynamic 3D *in silico* reconstructions will be useful to biologists. The three dimensional information in MPW images is evident by direct observation. However, rapid optical sectioning through reflection-space provides a thoroughly sampled dataset for 3D reconstruction. Within working distance limits, a sample anywhere in the imaging volume of the well can be seen in the reflections of each mirror simply by adjusting the focal depth (**Fig 2B,D**). Existing deconvolution techniques and 3D reconstruction methods applied to MPW z-sectioned data are likely to provide very accurate 3D models since each image acquisition gives multiple tilted views of the sample at the same point in time. A model that incorporates accurate spatial information over time may contain information that is not evident in simple 2D images. **Figure 3A and B** are fluorescent images at zero and 54 seconds in a time-series acquisition of a *Dictyostelium* cell stably transfected with GFP-tubulin (40X 1.3NA). The bright centrosome is visible in the alpha (α) image (**Fig 3Ai**) as well as primary (γ,ε) and secondary (γ-β,ε-β) (not shown) reflected images. The centrosome migrates from the lower to upper hemisphere of the cell during acquisition (**Fig 3A**,**B** and see Supplementary movie **Fig3A**). Note that the movement of the centrosome in the z axis is detected without doing a z-stack, demonstrating the power of this approach. A bright field series of images at varying focal depths of another *Dictyostelium* cell show what cells look like from varying perspectives (**Fig 3C,D,E)**. Given today's sensitive cameras, fast acquisition rates and rapid microscope stepper motors, rapid z-sectioning will provide simultaneous tilted-view data for 3D reconstructions of live specimen.

We describe a new and simple method for obtaining 3D image data from microscope specimens. The MPWs can be made with any size opening, rectangular or square. The depth of the well and the dimensions of the bottom are then related by the wall angle and etch time. The MPWs should be compatible with many microscopy techniques including fluorescence lifetime imaging and fluorescence recovery after photobleaching (FRAP), and will provide precise optical access to any part of the cell. In addition to providing aesthetically pleasing side-view and 3D images, this technique will provide more accurate information for quantitative studies in numerous processes including cell division, immune cell synapse formation, cell motility and embryo development. Thousands of MPWs can be fabricated in an area of a few square millimeters making MPW technology compatible with (BioMEMS) devices, which can ultimately be used for high-throughput screening and drug discovery. Single molecule imaging methods may also benefit from the increased signal and the precise spatial localization afforded by the use of the MPWs(Betzig and et al). The MPW in **Fig 1A** is geometrically concave and introverted, meaning that the optical center is within the well, due to the etch angle of silicon. Extroverted wells are also geometrically concave, but have their optical center outside of the cavity formed by the well. We have constructed extroverted MPWs by replica molding of faceted and polished stainless steel rods, and have successfully imaged specimen that are physically located outside of the well (data not shown). We believe extroverted MPWs will extend the use of this technology to specimen on planar substrates that cannot be easily positioned within an introverted well such as highly motile single cells and cell monolayers on a coverslip.

ACKNOWLEDGEMENTS

This research has been funded in part by AFOSR grant FA9550-05-1-0349 and the Vanderbilt Institute for Integrative Biosystems Research and Education (VIIBRE). KTS wishes to acknowledge helpful conversations with Mats Gustafsson at the University of California San Francisco and Sanford Simon at The Rockefeller University, and the editorial assistance of VIIBRE staff.

AUTHOR CONTRIBUTIONS

This work was made possible by the cooperation of all authors whose contributions are roughly as follows. KTS, RSR and CJJ planned and conducted all imaging experiments. DAM and IAG designed and fabricated the MPW devices. JPW provided significant theoretical and mathematical insight leading to the images of Fig 1, and all of the work was completed in the laboratories of JPW or CJJ. KTS had the primary responsibility for designing and drafting the manuscript, and all other authors contributed to its design and editing.

REFERENCES

1. Abbe,E., (1873) *Beiträge zur theorie des mikroskops und der mikroskopischen wahrnehmung.* Arkiv Mikroskop Anat **9**, 413-468.

2. Agard,D.A. and Sedat,J.W., (1983) *3-dimensional architecture of a polytene nucleus*. Nature **302**, 676-681.

3. Bell,L. and Jeon,K., (1963) *Locomotion of Amoeba Proteus*. Nature **198**, 675-676.

4. Betzig,E. and et al, (2006) *Imaging intracellular fluorescent proteins at nanometer resolution*. Science **313**, 1642-1645.

5. Boocock,C.A., Brown,A.F., and Dunn,G.A., (1985) *A simple chamber for observing microscopic specimens in both top and side views*. Journal of Microscopy-Oxford **137**, 29-34.

6. Born M. and Wolf E., 1965. Principles of Optics Pergamon Press, London.

7. Bradl,J., Hausmann,M., Schneider,B., Rinke,B., and Cremer,C., (1994) *A versatile 2-pi-tilting device for fluorescence microscopes*. Journal of Microscopy-Oxford **176**, 211-221.

8. Cao,J., Usami,S., and Dong,C., (1997) *Development of a side-view chamber for studying cell-surface adhesion under flow conditions*. Annals of Biomedical Engineering **25**, 573-580.

9. Cogswell,C.J., Larkin,K.G., and Klemm,H.U., (1996) *Fluorescence microtomography: multiangle image acquisition and 3D digital reconstruction*. Proc.SPIE **2655**, 109-115.

10. Dong,C., Cao,J., Struble,E.J., and Lipowsky,H.W., (1999) *Mechanics of leukocyte deformation and adhesion to endothelium in shear flow*. Annals of Biomedical Engineering **27**, 298-312.

11. Gustaffson,T. and Wolpert,L., (1967) *Cellular movement and contact in sea urchin morphogenesis.* Biological reviews of the Cambridge Philosophical Society **42**, 327.

12. Gustafsson,M.G.L., Agard,D.A., and Sedat,J.W., (1999) *(IM)-M-5: 3D widefield light microscopy with better than 100 nm axial resolution*. Journal of Microscopy-Oxford **195**, 10-16.

13. Harris,A., (1969) *Initiation and propagation of ruffle in fibroblast locomotion*. Journal of Cell Biology **43**, A165.

14. Hell,S. and Stelzer,E.H.K., (1992) *Properties of a 4pi confocal fluorescence microscope*. Journal of the Optical Society of America a-Optics Image Science and Vision **9**, 2159-2166.

15. Hell,S.W., Schrader,M., and VanderVoort,H.T.M., (1997) *Far-field fluorescence microscopy with three-dimensional resolution in the 100-nm range*. Journal of Microscopy-Oxford **187**, 1-7.

16. Hlinka,J. and Sanders,F.K., (1972) *Real and reflected images of cells in profile .1. method for study of cell movement and adhesion*. Journal of Cell Science **11**, 221.

17. Leyton-Mange,J., Yang,S., Hoskins,M.H., Kunz,R.F., Zahn,J.D., and Dong,C., (2006) *Design of a side-view particle imaging velocimetry flow system for cell-substrate adhesion studies*. Journal of Biomechanical Engineering-Transactions of the Asme **128**, 271-278.

18. Lindek,S., Stefany,T., and Stelzer,E.H.K., (1997) *Single-lens theta microscopy - a new implementation of confocal theta microscopy*. Journal of Microscopy-Oxford **188**, 280-284.

19. Lindek,S., Swoger,J., and Stelzer,E.H.K., (1999) *Single-lens theta microscopy: resolution, efficiency and working distance*. Journal of Modern Optics **46**, 843-858.

20. Roth,K.E., Rieder,C.L., and Bowser,S.S., (1988) *Flexible-substratum technique for viewing cells from the side - some invivo properties of primary (9+0) cilia in cultured kidney epithelia*. Journal of Cell Science **89**, 457-466.

21. Sanders,E.J. and Prasad,S., (1979) *Observation of cultured embryonic epithelial-cells in side view*. Journal of Cell Science **38**, 305-314.

22. Shaw,P.J., (1990) *3-dimensional optical microscopy using tilted views*. Journal of Microscopy-Oxford **158**, 165-172.

23. Shaw,P.J., Agard,D.A., Hiraoka,Y., and Sedat,J.W., (1989) *Tilted view reconstruction in optical microscopy - 3-dimensional reconstruction of drosophila-melanogaster embryo nuclei*. Biophysical Journal **55**, 101-110.

24. Sheppard,C.J.R., (1995) *Fundamental reduction of the observation volume in far-field light-microscopy by detection orthogonal to the illumination axis - confocal theta-microscopy*. Optics Communications **119**, 693-695.

25. Stelzer,E.H.K. and Lindek,S., (1994) *Fundamental reduction of the observation volume in far-field light-microscopy by detection orthogonal to the illumination axis - confocal theta microscopy*. Optics Communications **111**, 536-547.

26. Strutt JW (Lord Rayleigh), (1879) Nature **8**, 261-274, 403-411, 477-486.

27. Trupke,M., Ramirez-Martinez,F., Curtis,E.A., Ashmore,J.P., Eriksson,S., Hinds,E.A., Moktadir,Z., Gollasch,C., Kraft,M., Prakash,G.V., and Baumberg,J.J., (2006) *Pyramidal micromirrors for microsystems and atom chips*. Applied Physics Letters **88**.

FIGURE LEGENDS

Figure 1: MPW and preliminary simultaneous, multiple vantage point and side-view images. **A)** SEM image of MPW **B)** 3D rendering of 45º MPW with pipped die **C)** Autofluorescent *Helianthus Annuus* pollen grain in MPW **D)** Pulled glass pipette with 25 μm bulbous tip in optical center of MPW demonstrating 5 simultaneous views from multiple vantage points **E)** Fluorescent image of pipette tip of panel D with rhodamine coating **F)** 100X composite image of live *Sacchromyces cerevisiae* cell – upper left of diagonal are cell and two reflections at first focal plane – lower left of diagonal are two reflections at a deeper focal plane.

Figure 2: MPW image nomenclature. Red pips and text indicate real object, blue indicates reflections. Perspective (**A,B**) and Top (**C,D**) view of MPW reflections for optically centered (**A,C**) and eccentric (**B,D**) specimen. α – primary image, β – bottom reflection, γ,δ – first set of opposing mirrors, ε,ϕ – second set of opposing mirrors (β images are obscured in **C** and **D** by α image). Secondary reflections such as a gamma-mirror image of a beta mirror image are denoted by both mirror labels (γ-β), or an epsilon mirror image of a gamma (ε-γ), and similarly for tertiary reflections.

Figure 3: Composite timed-acquisition MPW fluorescent images of GFP-tubulin in a *Dictyostelium* cell at zero **(A)** and 54 seconds **(B)** as the centrosome migrates from the lower to upper hemisphere of the cell (cartoon insets lower right). Red arrows indicate the mirror plane separating primary from secondary reflections. **(C-E)** Bright field α,γ,ε and ε-γ composite images of *Dictyostelium* cell with pseudopodial extension arising from the dorsal surface of the cell.